Numerical Heat Transfer, Part A: Applications: An International Journal of Computation and Methodology
Publication details, including instructions for authors and subscription information:
http://www.tandfonline.com/loi/unht20

Experimental Validation of the Multiple Absorption Coefficient Zonal Method (MACZM) in a Dynamic Modeling of a Steel Reheating Furnace

Boutros Ghannam [a], Maroun Nemer [a], Khalil El Khoury [b] & Walter Yuen [c]

[a] Mines ParisTech, CEP—Center for Energy and Process Studies, Paris, France

[b] Lebanese University, Roumieh, Lebanon

[c] University of California Santa Barbara, Santa Barbara, California, USA

Published online: 05 Oct 2010.

To cite this article: Boutros Ghannam , Maroun Nemer , Khalil El Khoury & Walter Yuen (2010): Experimental Validation of the Multiple Absorption Coefficient Zonal Method (MACZM) in a Dynamic Modeling of a Steel Reheating Furnace, Numerical Heat Transfer, Part A: Applications: An International Journal of Computation and Methodology, 58:7, 545-563

To link to this article: http://dx.doi.org/10.1080/10407782.2010.511989

Numerical Heat Transfer, Part A, 58: 545–563, 2010

ISSN: 1040-7782 print/1521-0634 online
DOI: 10.1080/10407782.2010.511989

Taylor & Francis
Taylor & Francis Group

EXPERIMENTAL VALIDATION OF THE MULTIPLE ABSORPTION COEFFICIENT ZONAL METHOD (MACZM) IN A DYNAMIC MODELING OF A STEEL REHEATING FURNACE

Boutros Ghannam[1], Maroun Nemer[1], Khalil El Khoury[2], and Walter Yuen[3]

[1]*Mines ParisTech, CEP—Center for Energy and Process Studies, Paris, France*

[2]*Lebanese University, Roumieh, Lebanon*

[3]*University of California Santa Barbara, Santa Barbara, California, USA*

In this work, the multiple absorption coefficient zonal method (MACZM) is being implemented and validated numerically. The method is demonstrated to be highly suitable for the analysis of radiative heat transfer in multidimensional inhomogeneous non-grey media. A uniform rectangular fine grid is considered and small CPU time is achieved. This makes the method of great interest for transient applications. The validity of the method is demonstrated in two steps. First, cases with simple geometry are considered and results are compared to results generated by direct numerical integration. Results are also generated by MODRAY, which is a source project based on an original method called the flux-planes approximation, and are shown to be equally accurate. Second, the case of a steel reheating furnace is considered. In a previous work, the furnace heat balance and temperature profiles were simulated using a finite difference computation approach and radiative exchange factors generated by MODRAY. Experiments were performed and results generated by the model were found to be in good agreement with experimental data. The radiative exchange factors are now recalculated with MACZM. They are shown to be very close to those generated by MODRAY. The comparison of the two methods clearly shows that MACZM is much faster for the calculation of the volume-volume radiative exchange factors on a uniform rectangular grid.

INTRODUCTION

The principal limitation of dynamic modeling is generally the time needed for calculations, especially when considerably time-consuming calculations have to be repeated at each time step. In the dynamic modeling of high-temperature media, determining radiative heat transfer is usually the main difficulty, because it can be too time consuming, especially in applications with absorbing, emitting, and/or scattering multidimensional media. This is the case in the modeling of steel reheating furnaces, where radiative heat transfer is preponderant. Direct integration of the radiative heat

Received 12 May 2010; accepted 12 July 2010.

Address correspondence to Boutros Ghannam, Mines ParisTech, CEP—Center for Energy and Process Studies 60, boulevard Saint-Michel – F – 75272, Paris Cedex 06, France. E-mail: boutros.ghannam@mines-paristech.fr

NOMENCLATURE

a	absorption coefficient of volume	S	surface
D	characteristic dimension of the surface and volume used in the definition of generic exchange factors (GEF)	$\overline{s_i g_J}$	surface-volume direct exchange factor
		$\overline{s_i s_J}$	surface-surface direct exchange factor
dS	surface element	V	volume
F_{12}	view factor between surfaces A_1 and A_2	ε	emissivity
		θ	angular coordinate
$\overline{g_i g_J}$	volume-volume direct exchange factor	λ	wavelength
		ρ	reflectivity
L_{em}	emission mean beam length	τ	optical thickness, transmittance
L_{ij}	distance between two surface elements dS_i and dS_j	ϕ	angular coordinate
		Subscripts	
L_t	transmission mean beam length	a, b, c, d	surface index
n_x	dimensionless x-coordinate	i, j, k, n, m	element index
n_y	dimensionless y-coordinate	pd	perpendicular component
n_z	dimensionless z-coordinate	pp	parallel component
N_ϕ	number of angular elements		

transfer equation is very difficult, even for relatively simple applications. Hence, many numerical methods have been developed over the years in order to approximate radiative heat transfers. Most of these methods, however, are too time consuming and therefore not applicable to dynamic modeling of practical systems.

The spherical harmonics method [1] is good for optically thick media, but it fails for large optical thicknesses ($\tau \gg 10$). The method also gives good results for media with near-isotropic radiative intensity. The spherical harmonics method is well adapted when grid refinement is necessary in order to obtain more accurate results.

The discrete ordinates method [2–4] has been used extensively for many multi-mode heat transfer fluid mechanics problems. The limitation of the method is false scattering and ray effect. In addition, the method does not ensure the conservation of energy. The finite-volume method, which is derived from the discrete-ordinate method [5–7], ensures the conservation of energy. However, it can be very time consuming in optical thick media.

The Monte Carlo method [8, 9] is a statistical method and is totally stochastic. Its advantage is that it can be used for complex geometries and it does not include any approximations, contrary to other methods. It is well suited for handling spectral radiation. Its accuracy depends on the number of statistical operations, which consists of tracing a large number of photons from their points of emission to their points of attenuation in the enclosure. The limitation of this method is the huge time of calculation. The large CPU time makes the method only suitable for verification purposes.

The discrete transfer method [10] combines the previous two methods and the zonal method. It is based on ray tracing. Rays from a large number of points on the enclosure surfaces are emitted in all directions similarly to the Monte Carlo method. The amount of energy supported by the ray is then evaluated. This method, however, has the same shortcomings as the discrete-ordinate method and is more time consuming.

The zonal method [11–13] was originally developed by Hottel and Sarofim over 30 years ago. It is considered a very accurate method for modeling multidimensional

radiative heat transfer in homogeneous and isothermal media. The concept of generic exchange factor [13] and superposition are introduced to generalize the method for absorbing, emitting, and/or scattering multidimensional medium with complex geometry. The accuracy of the method depends on grid size. Nevertheless, the definition of generic exchange factors is unable to simulate correctly the physics of a general inhomogeneous medium, even if a finer grid is considered [14].

Multiple absorption coefficient zonal method (MACZM) is based on the concept of generic exchange factors similarly to the traditional zonal method. However, a new definition of generic exchange factors is introduced by Yuen [14] in order to better simulate the physics of radiative heat transfer in inhomogeneous non-isothermal media. The method has been shown to be efficient and accurate in simulating radiative heat transfer in a two-phase inhomogeneous media [14] found in a numerical simulation of steam explosion. In the MACZM, the generic exchange factor has been expanded to a two-component formulation in order to account for the possibility of large variation of absorption coefficient in regions surrounding the absorbing or emitting volume elements. Accordingly, the conventional unique absorption coefficient exchange factor of the zonal method is replaced by a set of three absorption coefficients volume-volume exchange factors and two absorption coefficients volume-surface exchange factors. In its first application [14], these exchange factors were tabulated and applied to calculate radiative heat transfer in a two phase medium. As a simplification of the approach, a set of six mean beam lengths are defined in a mathematically self-consistent manner [15], and they are used to calculate exchange factors instead of using tabulated tables.

The objective of the present work is to demonstrate the validity of MACZM with two examples. First, the method will be used to generate the set of exact elementary exchange factors given by Yuen and Takara [13]. Another calculation tool called MODRAY is also described. It is based on the flux-planes method of El Khoury that was briefly presented in reference [16] and is used for the calculation of radiative exchange factors. MODRAY results are also presented in comparison with the exact results given by Yuen and Takara [13].

In the second example, a semi-industrial steel reheating furnace previously modeled and experimentally tested by Ferrand [17] is presented. The furnace is equipped with two flameless oxidation regenerative burners. The furnace geometry and gas distribution are described, and a CFD approach for the representation of the burners in the simulations is briefly discussed. In order to estimate the radiative heat transfer, the direct exchange factors are generated by both MODRAY and MACZM and compared. The heat balances and temperature profiles in the furnace are simulated dynamically, using the exchange factors calculated by MODRAY. Results of experimental tests for temperature profiles and heat balances in the furnace are taken from Ferrand [17] and compared to simulations for the validation of both MODRAY and MACZM.

MULTIPLE ABSORPTION COEFFICIENT ZONAL METHOD (MACZM)

Concept of Generic Exchange Factors (GEF) and Superposition

The basis of the zonal method is the concept of generic exchange factor (GEF) [14]. A generic exchange factor corresponds to the fraction of energy emitted from one radiating element and absorbed by another, the element being an elementary

volume or elementary surface. Yuen [14] has introduced the definition of three "2-components" partial generic exchange factors. The total GEFs are then deduced by superposition of partial generic exchange factors. The concept of partial generic exchange factors and superposition are discussed in detail by Yuen [14], and they will now be briefly presented.

A mesh consisting of a uniform rectangular grid is the basic geometry used by MACZM. The relevant geometry is thus composed from elementary cubes or voxels. The position of a voxel is referred by the coordinates of its bottom left corner. The radiative exchange between two volume elements is characterized by two partial exchange factors; a parallel component $(g_1g_2)_{pp}$ and a perpendicular component $(g_1g_2)_{pd}$ (Figure 1). $(g_1g_2)_{pp}$ corresponds to the fraction of the volume to volume radiative exchange which passes through the top surface of V_1 and the bottom surface of V_2, and $(g_1g_2)_{pd}$ corresponds to the fraction that passes through the x-direction side surface of V_1 and the bottom surface of V_2. The two partial volume-volume exchange factors are expressed in a dimensionless form as a function of three optical thicknesses (a_1D, a_2D, a_mD), and the dimensionless separation between the two volume elements (n_x, n_y, n_z).

$$\frac{(g_1g_2)_{pp}}{D^2} = F_{ggpp}(a_1D, a_2D, a_{m,zz}D, n_x, n_y, n_z) \tag{1}$$

$$\frac{(g_1g_2)_{pd}}{D^2} = F_{ggpd}(a_1D, a_2D, a_{m,xz}D, n_x, n_y, n_z) \tag{2}$$

where D is the voxels dimension, a_1 and a_2 are the mean absorption coefficients inside volumes V_1 and V_2 respectively, and a_m the average absorption coefficient along the center to center line of sight between the two surfaces through which the radiation passes. The actual volume-volume exchange factor is generated by the superposition of nine partial volume-volume exchange factors.

Two partial volume–surface exchange factors $(g_1s_2)_{pp}$ and $(g_1s_2)_{pd}$ are expressed in a similar manner (Figure 2). The volume–surface exchange factors are thus a function of two optical thicknesses (a_1D, a_mD) and the dimensionless separation between

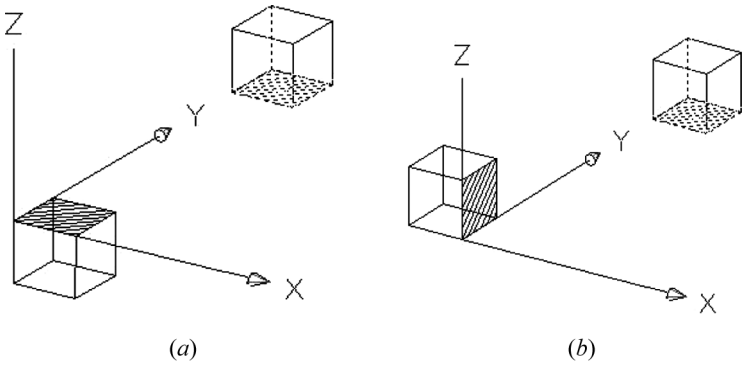

(*a*) (*b*)

Figure 1. Volume-volume GEFs. (*a*) Parallel component and (*b*) perpendicular component.

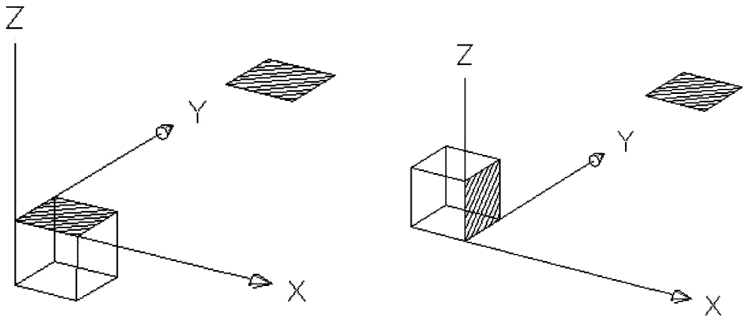

(*a*) (*b*)

Figure 2. Volume-surface GEFs. (*a*) Parallel component and (*b*) perpendicular component.

the two volume elements.

$$\frac{(g_1 s_2)_{pp}}{D^2} = F_{gspp}(a_1 D, a_{m,zz} D, n_x, n_y, n_z) \tag{3}$$

$$\frac{(g_1 s_2)_{pd}}{D^2} = F_{gspd}(a_1 D, a_{m,xz} D, n_x, n_y, n_z) \tag{4}$$

The parallel component $(g_1 s_2)_{pp}$ corresponding to the fraction of the radiative exchange, which passes through the top surface of the volume V_1, and the perpendicular component $(g_1 s_2)_{pd}$ corresponding to the fraction that passes through the x-direction side surface of V_1. The superposition of three volume-surface partial generic exchange factors gives the volume-surface exchange factor.

Finally, the parallel and perpendicular surface–surface exchange factors are functions of only one average absorption coefficient for the intervening medium,

$$\frac{(s_1 s_2)_{pp}}{D^2} = F_{sspp}(a_{m,zz} D, n_x, n_y, n_z) \tag{5}$$

$$\frac{(s_1 s_2)_{pd}}{D^2} = F_{sspd}(a_{m,xz} D, n_x, n_y, n_z) \tag{6}$$

In Yuen [14], partial generic exchange factors were tabulated. MACZM can then be applied to a uniform rectangular grid, and the partial generic exchange factors are directly taken from tables, which require quite a large computer memory. However, while the partial exchange factors are tabulated for a finite number of inputs, interpolations need to be performed in order to find partial exchange factors corresponding to a set of variables situated in the interval between the tabulated points. This leads to an inevitable small error.

Mean Beam Length (MBL) and Artificial Neural Network Correlations

In a recent work, Yuen [15] has defined a set of mean beam lengths that allow partial generic exchange factors to be written in a one-dimensional form as functions

of these mean beam lengths. Six MBLs were defined in order to provide a correct length scale to account for three-dimensional surface-surface, surface-volume, and volume-volume radiative heat transfer. Similarly to partial GEFs, MBLs are defined between two elements (volumes or surfaces), and they are also functions of the three optical thicknesses (a_1D, a_2D, a_mD) and the dimensionless separation between the two elements (n_x, n_y, n_z). In the present work, MACZM is being implemented together with the MBL functions, in one single code. The partial generic exchange factors in the code are then given by the corresponding functions of MBLs, instead of being read from tables, leading to better computational speed and numerical accuracy.

Mean beam lengths are discussed in detail by Yuen [15], and they are now briefly summarized. Transmission mean beam length is physically equivalent to the one-dimensional path length that gives the same transmission of radiation propagated between two surfaces through the considered medium. It is related mathematically to the two surface-surface GEFs, by the following equations.

$$\frac{(s_1 s_2)_{pp}}{D^2} = F_{12,pp}(n_x, n_y, n_z) e^{-a_m L_{t,pp}} \tag{7}$$

$$\frac{(s_1 s_2)_{pd}}{D^2} = F_{12,pd}(n_x, n_y, n_z) e^{-a_m L_{t,pd}} \tag{8}$$

where $L_{t,pp}$ and $L_{t,pd}$ are parallel and perpendicular transmission MBLs, and $F_{12,pp}$ *and* $F_{12,pd}$ the form factors between the two surfaces.

Similarly, emission mean beam length is interpreted physically as the equivalent one-dimensional path length that gives the same emissivity as the emitting volume. The extension of the previous two equations gives the relation between the emission mean length and the volume-surface GEFs.

$$\frac{(g_1 s_2)_{pp}}{D^2} = F_{12,pp}(n_x, n_y, n_z)(1 - e^{-a_1 L_{em,pp}}) e^{-a_m L_{t,pp}} \tag{9}$$

$$\frac{(g_1 s_2)_{pd}}{D^2} = F_{12,pd}(n_x, n_y, n_z)(1 - e^{-a_1 L_{em,pd}}) e^{-a_m L_{t,pd}} \tag{10}$$

where $L_{em,pp}$ and $L_{em,pd}$ are the parallel and perpendicular emission MBLs.

Absorption mean beam length is interpreted physically as the equivalent one-dimensional path length that gives the same absorption as the absorbing volume. The relation between the volume-volume GEFs are then given by

$$\frac{(g_1 g_2)_{pp}}{D^2} = F_{ggpp} = F_{12,pp}(n_x, n_y, n_z)(1 - e^{-a_2 L_{a,pp}})(1 - e^{-a_1 L_{em,pp}}) e^{-a_m L_{t,pp}} \tag{11}$$

$$\frac{(g_1 g_2)_{pd}}{D^2} = F_{ggpd} = F_{12,pd}(n_x, n_y, n_z)(1 - e^{-a_2 L_{a,pd}})(1 - e^{-a_1 L_{em,pd}}) e^{-a_m L_{t,pd}} \tag{12}$$

$L_{a,pp}$ and $L_{a,pd}$ being the parallel and perpendicular absorption.

Since simple mathematical algebraic correlations for MBLs are difficult to be obtained, two layers artificial neural network correlations were generated in order to estimate the MBLs. The sufficient number of neurons for each case is taken in order to obtain a relative error of less than 5%. Numerical data used in the neural network training process are generated for a limited range of input variables; neural network is then generated for the same range of inputs. The optical thicknesses $a_1 D$, $a_2 D$, and τ vary between 0.01 and 4.6 in all cases. The dimensionless distances n_x, n_y, and n_z are different for each case, but their values remain always less than eight. For optical thicknesses greater than 4.6, the volume approaches a black body and in large distance limits GEF is sufficiently small such that the accuracy of MBL does not contribute significantly to the heat transfer simulation. Specifically, when the optical thickness exceeds 4.6, the MBL is taken to be identical to the value with an optical thickness of 4.6. When the dimensionless distances are out of the input range, the MBL for the closest distance inside the limits is taken. More detail about the artificial neural network correlations can be found in Yuen [15].

MODRAY TOOL DESCRIPTION

MODRAY calculates the total exchange factors for the zonal method in three steps. First, the surface-surface direct exchange factors are calculated with the flux-planes method. Second, the surface-volume and volume-volume direct exchange factors are deduced by conservation considerations. Last, the total exchange factors are calculated by a generalized version of the plating algorithm.

Calculation of Direct Exchange Factors $\overline{s_i s_j}$ with the Flux Planes Method

The flux-planes method is based on an angular formulation of the direct exchange factors. The formulas are then calculated numerically after a discretization of the flux outgoing from an elemental surface by quarter-planes called the flux planes. The method is briefly described here.

Consider an elemental area dS_i of surface S_i centered on point M. As seen from M, a surface S_j is situated between ϕ_1 and ϕ_2 in the ϕ direction, and between θ_1 and θ_2 for each value of θ (Figure 3*a*). In an absorbing/nonscattering medium, the radiation heat transfer rate that reaches S_j from dA_i is

$$dq_{ij} = \int_{\phi_1}^{\phi_2} \int_{\theta_1(\phi)}^{\theta_2(\phi)} I_i \tau_{ij} \sin\theta \cos\theta \, d\theta \, d\phi \tag{13}$$

where I_i is the constant intensity of the isotropic radiation leaving dS_i, and τ_{ij} is the mean transmittance between dS_i and S_j in the path of direction (ϕ, θ). If the path goes through M, different volumes with different absorption coefficients a_m ($m = 1, M$) and has a length L_m in each one, then

$$\tau_{ij} = \exp\left(-\sum_{m=1}^{M} a_m L_m\right) \tag{14}$$

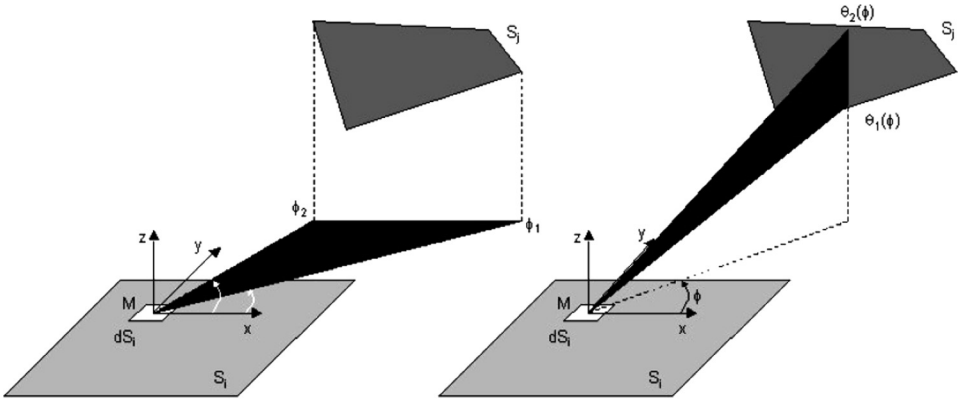

(*a*)

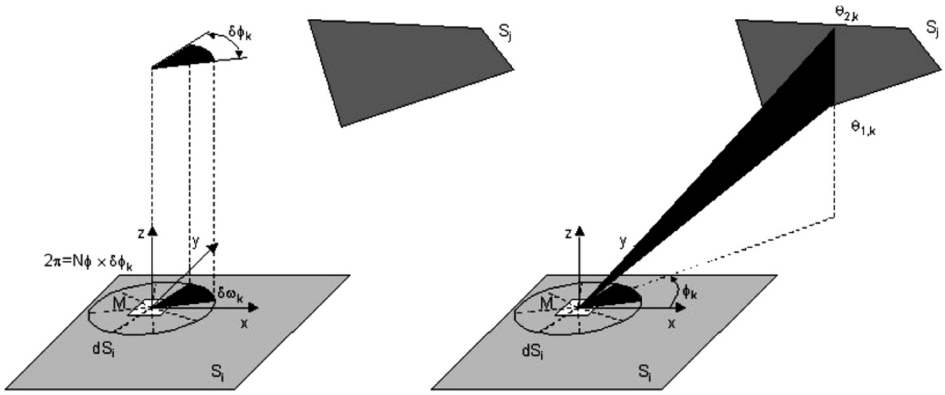

(*b*)

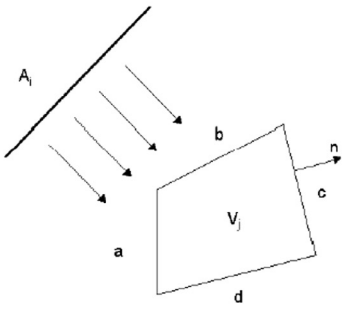

(*c*)

Figure 3. Geometry of direct exchange factors calculation in MODRAY. (*a*) Limits of a surface as seen from point M; (*b*) flux planes approximation; and (*c*) calculation of surface-volume and volume-volume factors from surface-surface ones.

Knowing that the heat flux leaving dS_i in all directions is equal to πI, and after integration on S_i, the angular formulation of the direct exchange factor between S_i and S_j will be

$$\overline{s_i s_j} = \frac{1}{2\pi} \int_{s_i} \int_{\phi_1}^{\phi_2} \int_{\theta_1(\phi)}^{\theta_2(\phi)} \tau_{i,j} d(\sin^2 \theta) d\phi dS_i \tag{15}$$

The hemisphere surrounding the point M of the elemental surface dS_i can be decomposed into a finite number of partitions N_ϕ with equal solid angles $\delta\omega_k (k = 1, N_\phi)$, each included between two quarter-plane normal to dS_i, and making an angle $\delta\phi_k$ equal to $2\pi/N_\phi$.

The radiative flux dq_i leaving the surface dS_i is then equal to the sum of the fluxes $dq_{i,k}$ leaving point M through the solid angles $\delta\omega_k (k = 1, N_\phi)$. The flux-planes approximation consists in considering that each flux $dq_{i,k}$ is concentrated in the bisector plane of $\delta\omega_k$ (Figure 3*b*). Thereafter, Eq. (15) reduces to

$$\overline{s_i s_j} \frac{1}{N_\phi} \int_{s_i} \left(\sum_{k:\phi_1 \le \phi_k \le \phi_2} \int_{\theta_1(\phi)}^{\theta_2(\phi)} \tau_{ij} d(\sin^2 \theta) dS_i \right) \tag{16}$$

where $\theta_{1,k}$ and $\theta_{2,k}$ are the angular limits of S_i in the direction of the bisector plane. Both integrals in Eq. (16) are calculated by a Gaussian quadrature.

Calculation of Surface-Volume and Volume-Volume Direct Exchange Factors using Emery et al. Relations

Emery et al. have demonstrated that surface-volume and volume-volume exchange factors can be deduced from surface-surface ones using conservation considerations, and the fact that each volume is bounded by surfaces. The whole approach is discussed in detail in Emery et al. [18]. In the example of Figure 3*c*, we have,

$$\overline{s_i g_j} = \overline{s_i s_a} + \overline{s_i s_b} - \overline{s_i s_c} - \overline{s_i s_d} \tag{17}$$

Calculation of Total Exchange Factors using the Plating Algorithm

Once the direct exchange factors are calculated by MODRAY or MACZM, Edwards plating algorithm [19–21] is applied in order to find the total exchange factors by using a set of recursion relations. Starting from the direct exchange areas named $\overline{\boldsymbol{ss}}^{(0)}$, $\overline{\boldsymbol{sg}}^{(0)}$, $\overline{\boldsymbol{gs}}^{(0)}$, and $\overline{\boldsymbol{gg}}^{(0)}$ the total exchange areas is obtained after plating the N surfaces in the enclosure and correspond to $\overline{\boldsymbol{ss}}^{(N)}$, $\overline{\boldsymbol{sg}}^{(N)}$, $\overline{\boldsymbol{gs}}^{(N)}$, and $\overline{\boldsymbol{gg}}^{(N)}$. After the plating of surface S_k, the exchange areas have to be changed according to

$$\overline{s_k s_k}^{(k)} = C_k A_k \varepsilon_k^2 \overline{s_k s_k}^{(k-1)} \tag{18}$$

$$\overline{s_i s_k}^{(k)} = C_k A_k \varepsilon_k \overline{s_i s_k}^{(k-1)} \tag{19}$$

$$\overline{s_k s_j}^{(k)} = C_k A_k \varepsilon_k \overline{s_k s_j}^{(k-1)} \tag{20}$$

$$\overline{g_i s_k}^{(k)} = C_k A_k \varepsilon_k \overline{g_i s_k}^{(k-1)} \tag{21}$$

$$\overline{s_k g_i}^{(k)} = C_k A_k \varepsilon_k \overline{s_k g_i}^{(k-1)} \tag{22}$$

$$\overline{s_i s_j}^{(k)} = \overline{s_i s_j}^{(k-1)} + C_k \rho_k \overline{s_i s_k}^{(k-1)} \overline{s_k s_j}^{(k-1)} \tag{23}$$

$$\overline{s_i g_j}^{(k)} = \overline{s_i g_j}^{(k-1)} + C_k \rho_k \overline{s_i s_k}^{(k-1)} \overline{s_k g_j}^{(k-1)} \tag{24}$$

$$\overline{g_i s_j}^{(k)} = \overline{g_i s_j}^{(k-1)} + C_k \rho_k \overline{g_i s_k}^{(k-1)} \overline{s_k s_j}^{(k-1)} \tag{25}$$

$$\overline{g_i g_j}^{(k)} = \overline{g_i g_j}^{(k-1)} + C_k \rho_k \overline{g_i s_k}^{(k-1)} \overline{s_k g_j}^{(k-1)} \tag{26}$$

with

$$C_k = \frac{1}{A_k - \rho_k \overline{s_k s_k}^{(k-1)}} \tag{27}$$

ELEMENTARY OPERATIONS VALIDATION

Direct exchange factors were calculated by direct numerical integration and tabulated by Yuen and Takara [13]. The authors have estimated the relative difference from the exact solution to be less than 1%. In order to validate the two approaches, MACZM and MODRAY, exchange factors generated by these two methods are compared to the tabulated factors of Yuen and Takara [13].

Four direct transfer factors, $\overline{gg}$, $\overline{gs}$, $\overline{ss}_p$, and $\overline{ss}_t$ are calculated. The geometry of the four cases is represented in Figure 4 and is described in detail in Yuen and Takara [13]. Three different geometric configurations are considered and the corresponding transfer factors are calculated using MACZM and MODRAY. In all cases, the absorption coefficient inside the enclosure is considered to be constant with a value of $0.5\,\mathrm{m}^{-1}$. The values generated by MACZM and MODRAY as well as the tabulated ones of Yuen and Takara are presented together in Table 1.

It can be readily observed that MACZM is generally quite accurate (with a relative error of less than 5%) for exchange factors with values greater than 0.001. Larger relative errors occur when the value of exchange factor becomes small, and the error generally increases as the magnitude of the exchange factor becomes

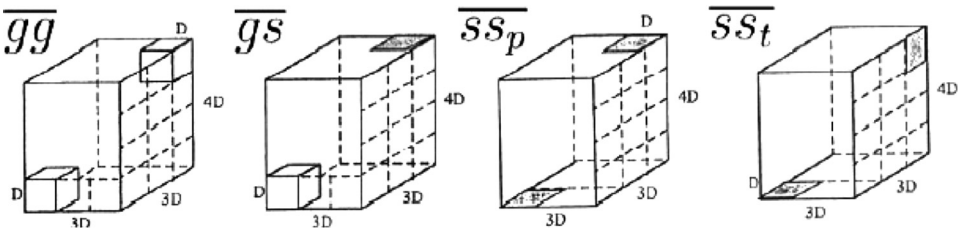

Figure 4. Geometry of exchange factors represented in Table 1.

Table 1. Comparison between some dimensionless exchange factors generated by MACZM (the first row), those generated by Modray using the flux planes method (the second row), and values tabulated by Yuen and Takara (in parentheses)

		MACZM – MODRAY (Yuen & Takara) [Relative difference]					
gg	$N_iN_jN_k$	$\kappa D = 0.2$	Δ[%]	$\kappa D = 1.0$	Δ[%]	$\kappa D = 4.0$	Δ[%]
	113	2.3154E-03	4.2	1.3378E-02	2.1	1.7203E-03	0.7
		2.3717E-03	6.7	1.3049E-02	0.4	1.7323E-03	0.1
		(2.2228E-03)		(1.3100E-02)		(1.7344E-03)	
	223	1.3839E-03	0.3	5.6961E-03	2.9	1.8741E-04	19.1
		1.5015E-03	8.8	5.5715E-03	0.7	2.3206E-04	0.2
		(1.3796E-03)		(5.5350E-03)		(2,3168E-04)	
	435	1.5581E-04	14.3	5.9767E-05	5.1	1.5242E-10	52.8
		1.4947E-04	9.6	5.7145E-05	0.5	2.9283E-10	9.3
		(1.3636E-04)		(5.6840E-05)		(3.2288E-10)	
gs	$N_iN_jN_k$	$\kappa D = 0.2$	Δ[%]	$\kappa D = 1.0$	Δ[%]	$\kappa D = 4.0$	Δ[%]
	113	5.8736E-03	0.0	4.1738E-03	4.5	1.5196E-05	4.2
		5.9426E-03	1.1	4.1704E-03	4.4	1.5207E-05	4.3
		(5.8780E-03)		(3.9950E-03)		(1.4580E-05)	
	223	3.7726E-03	0.25	2.0345E-03	1.4	2.6680E-06	11.4
		3.7607E-03	0.6	2.0241E-03	1.9	3.1777E-06	5.5
		(3.7820E-03)		(2.0640E-03)		(3.0116E-06)	
	435	4.7446E-04	1.4	2.4771E-05	0.12	4.2492E-11	27.5
		4.7416E-04	1.3	2.5148E-05	1.4	7.0104E-12	19.6
		(4.6800E-04)		(2.4800E-05)		(5.8600E-12)	
ss_p	$N_iN_jN_k$	$\kappa D = 0.2$	Δ[%]	$\kappa D = 1.0$	Δ[%]	$\kappa D = 4.0$	Δ[%]
	113	1.7915 E-02	2.2	1.5528E-03	0.46	1.5809E-07	5.2
		1.7913E-02	2.2	1.5601E-03	0.0	1.6688E-07	0.0
		(1.7530E-02)		(1.5600E-03)		(1.6680E-07)	
	223	1.1842E-02	0.78	8.4290E-04	0.67	4.2831E-08	7.7
		1.1831E-02	0.7	8.3660E-04	0.1	4.6376E-08 0.0	0.0
		(1.1750E-02)		(8.3730E-04)		(4.6390E-08)	
	435	1.6144E-03	0.27	1.2128E-05	0.48	1.2917E-13	23.7
		1.6116E-03	0.1	1.2020E-05	0.4	1.6259E-13	4.0
		(1.6100E-03)		(1.2070E-05)		(1.6930E-13)	
ss_t	$N_iN_jN_k$	$\kappa D = 0.2$	Δ[%]	$\kappa D = 1.0$	Δ[%]	$\kappa D = 4.0$	Δ[%]
	113	5.3625E-03	0.65	7.2742E-04	0.26	4.4655E-07	22.7
		5.2217E-03	2.0	7.1113E-04	2.5	5.6619E-07	2.0
		(5.3280E-03)		(7.2930E-04)		(5.7770E-07)	
	223	7.0203E-03	1.1	6.3247E-04	0.59	8.1960E-08	34.7
		7.1190E-03	2.5	6.4590E-04	1.5	1.2934E-07	3.0
		(6.9470E-03)		(6.3620E-04)		(1.2560E-07)	
	435	1.1217 E-03	0.38	9.2422E-06	2.1	1.3947E-13	44.9
		1.1362E-03	0.9	9.1107E-06	3.5	2.3777E-13	6.1
		(1.1260E-03)		(9.4410E-06)		(2.5330E-13)	

smaller (e.g., the error is 52.8% for $\overline{gg(4,3,5)}$). However, for practical applications, the large relative error for the small exchange factor (with values less than 0.001) is not significant since it will have a negligible impact on the overall energy balance. Values generated by MODRAY are also found to be in good agreement with exact ones for all optical thicknesses. MODRAY is thus shown to give accurate results; it can be used, then, in the next section for comparisons with MACZM before performing the experimental validation.

TEST CASE DESCRIPTION

Furnace Description

The experimentations were carried out by Ferrand [17] on a steel reheating test furnace designed at semi-industrial scale. The outside and inside views of the furnace are shown in Figure 5. Its internal dimensions are 300 cm × 160 cm × 110 cm. It is equipped with two HRS-DL 200 kW flameless oxidation regenerative burners from the NFK Company (Japan), placed in the upper zone of the furnace. A slab of conventional carbon steel having the dimensions 100 cm × 100 cm × 22 cm can be introduced into the furnace and laid on four bases made of refractory concrete. The walls are multilayered with refractory material from inside and insulation from outside.

Modeling Approach

The whole system is modeled as a network of interacting components, each having its own internal model. The slab is divided into 16 one-dimensional components, each having a cross-section of 25 cm × 25 cm and a length of 22 cm, and modeled with finite elements. The thermal conduction in the other two dimensions is taken into account by simple lateral exchange coefficients. The walls are modeled with one-dimensional finite elements in the inside-outside direction. Each concrete base is modeled with two finite volumes. As for the gases, they are modeled as four separate zones, taking into account the different levels of temperature—and consequently different gas properties—and the heat generation process. A detailed CFD study performed by Ferrand [17] showed that each combustion zone could be represented by a simple parallelepiped of dimensions 100 cm × 28 cm × 28 cm with uniform temperature and heat generation rate. The rest of gases are represented by two zones; an upper zone and a lower zone. The radiation heat exchanges are modeled by the zonal method with total transfer factors calculated via the plating algorithm from the direct exchange factors generated by MODRAY. A sensitivity study showed that a simple grey gas model could be a reasonable approximation in the modeling of the reheat furnace. More detail about the modeling approach can be found in Ferrand [17].

(*a*) (*b*)

Figure 5. Semi-industrial furnace. (*a*) Outside view and (*b*) inside view.

Test Procedure

Tests were performed on the furnace in order to provide experimental data for validating the simulation model. The burners are equipped with all the necessary measurement devices to provide the complete heat balance of the system. The heat flows and temperatures corresponding to the fresh air and combustion gases are measured, as well as the regenerative cell temperatures from its cold and hot sides. Heat flow rates are deduced from temperature differences, and temperatures are measured by thermocouples of types S and K. While a precise knowledge of the temperature profiles in the furnace is important for the validations, 19 measurement points were taken. They are placed where high temperature gradients are expected, which are estimated based on CFD calculation results. The slab temperature is measured in 12 different points (Figure 6). Thermocouples are introduced via horizontal or vertical holes in the slab depending on their locations.

In the operating mode, the furnace temperature is raised up and stabilized at 1300°C before the slab is introduced. When the slab is introduced into the furnace, the burners operating power is at its maximum. The slab is taken outside to the furnace after approximately two hours. It is cooled in ambient air until its surface temperature reaches 500°C, and is then reintroduced into the furnace. When the steel slab temperature reaches the desired set temperature (1200°C), it is finally taken out of the furnace.

All tests were performed by Ferrand [17], and they are used here for experimental validation. The heat balance and efficiency profiles as well as the slab and enclosure temperature profiles, are evaluated.

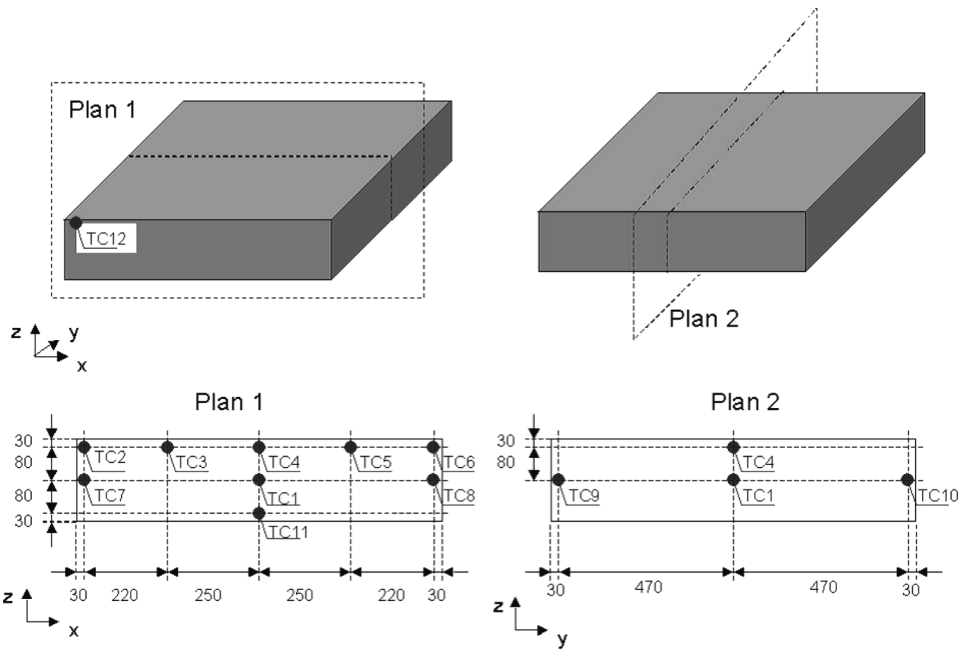

Figure 6. Positions of the thermocouples inside the slab of steel.

CALCULATION OF RADIATIVE EXCHANGE FACTORS

Calculation of the Direct Exchange Factors in the Furnace using MACZM

The furnace as described in the previous paragraph, is modeled using MACZM for the evaluation of direct radiative heat transfer factors. The volume mesh of the scene and objects are shown in Figure 7. Burners are represented by two parallelepipeds (100 cm × 28 cm × 28 cm) in the upper zone with 60 cm separating distance between them. Based on the CFD study, the furnace is totally filled with combustion gases that are supposed to be grey gases with an absorption coefficient of $0.4\,m^{-1}$, as well as the combustion volumes, which are also modeled as grey gases having an absorption coefficient of $0.4\,m^{-1}$. The absorption coefficient is thus constant in the whole volume in this case; variable absorption coefficient in the space can be similarly treated and the time of calculation is not influenced. The mesh applied to the furnace has a voxel dimension of $10\,cm^3$, which generates $30 \times 16 \times 11$ voxels.

Calculation of the Direct Exchange Factors using MODRAY

The direct transfer factors for radiation heat transfer are also generated by MODRAY. The same furnace geometry and properties are considered. As described previously, in MODRAY there is no volume meshing. Three different cases of surface meshing are considered.

1. Scene $6 \times 6 \times 6$, slab of steel $12 \times 12 \times 4$, combustion volume $2 \times 2 \times 2$, bases $2 \times 2 \times 2$
2. Scene $4 \times 4 \times 4$, slab of steel $6 \times 6 \times 2$, combustion volume $2 \times 2 \times 2$, bases $2 \times 2 \times 2$
3. Scene $2 \times 2 \times 2$, slab of steel $6 \times 6 \times 2$, combustion volume $2 \times 2 \times 2$, bases $2 \times 2 \times 2$

The furnace meshing of case 1 is shown in Figure 8.

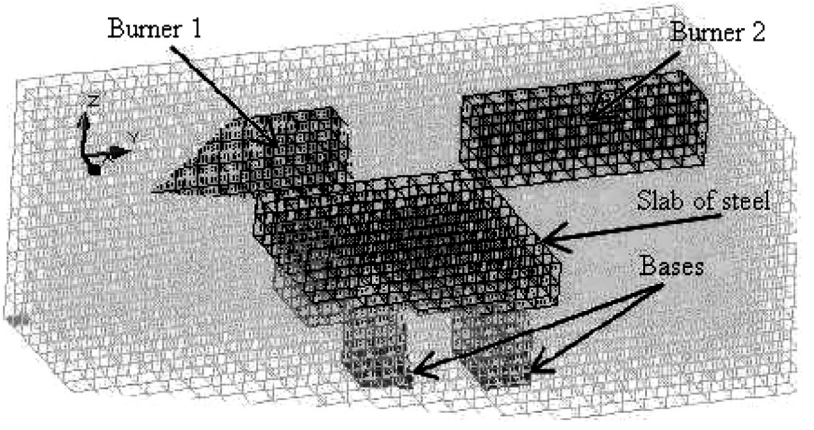

Figure 7. Volume meshing of the furnace (MACZM).

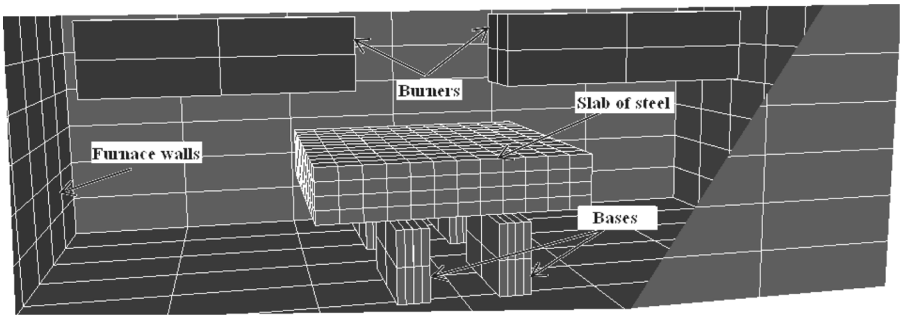

Figure 8. Surface meshing of the furnace (MODRAY).

Comparison of Results and Discussion

The direct exchange factors calculated by MACZM and MODRAY are shown together in Table 2. Exchange factors corresponding to the three basic radiative exchange processes (volume-volume, volume-surface, and surface-surface) are considered. In general, MACZM generates the exchange factors accurately and efficiently. With a mesh size of 10 mm × 10 mm × 10 mm, two-second calculation time is sufficient, with the same accuracy level as MODRAY, which requires computational time of 2 min, 6–7 min, and 25 min for the considered grid sizes.

The mesh of MODRAY case 1 is the finer and as expected, it has the highest level of accuracy compared to cases 2 and 3. The time of calculation is in the range of 2 min in case 3 to 25 min in case 1. The calculation time is then higher than in MACZM, especially with a fine mesh. Nevertheless, when a finer mesh is considered in MODRAY the summation in Eq. (16) approaches the actual integral, and then the solution approaches the exact solution, noting that at the other side, MACZM accuracy is independent of mesh size as demonstrated by Yuen [14]. Factors generated by MACZM are found to be in high agreement with MODRAY case 1, in volume-volume, and volume-surface exchanges. A slight difference in the case of surface-surface exchange factors (exchange between base $\boldsymbol{a_{int}}$ and base $\boldsymbol{b_{int}}$) is

Table 2. Comparison between direct exchange factors generated by MODRAY and MACZM, and time of calculation

Comparison MACZM – MODRAY				
Direct exchange factors [Calculation run time]	MACZM [2 sec]	MODRAY 1 [25 min]	MODRAY 2 [6–7 min]	MODRAY 3 [2 min]
Combustion volume(1)-combustion volume(2)	1.13560E-04	9.98015E-05	1.18587E-04	1.27992E-02
Combustion volume(1)-steel slab	1.03177E-02	1.00157E-02	9.76513E-03	8.68062E-02
Combustion volume(2)-steel slab	1.04588E-02	1.01281E-02	9.95802E-03	8.56366E-02
Base a_{int}–Base b_{int}	3.28529E-02	3.09024E-02	3.08996E-02	3.09022E-02

observed. It is due to the fact that the volume meshing used in MACZM does not perfectly match the geometry of the bases.

High agreement is observed between the results generated by MACZM code and MODRAY case 1. The accuracy of the two methods is thus demonstrated. The solution in MODRAY approaches the real one when a finer mesh is considered; nevertheless the time is considerably increased. The advantage of MODRAY is that the meshing can be applied to any geometry, while in MACZM the geometry of objects in the scene has to agree with the rectangular structured mesh. When the object geometry is not rectangular, error can occurs as seen in the last line of Table 2 and a smaller mesh size will be needed to improve accuracy.

EXPERIMENTAL VALIDATION

In Figure 9, the simulation and experimental temperature profiles of the furnace ceiling over the whole cycle are shown. At the beginning, the furnace temperature is stabilized at 1300°C before the slab of steel is introduced. When the slab is introduced, the ceiling temperature decreases rapidly. It again reaches the set value of 1300°C during the phase when the slab is taken out of the furnace. Another temperature decrease is observed when the slab is finally reintroduced into the furnace. The relative difference between the simulated and measured temperatures of the furnace ceiling is less than 1% during the whole procedure.

The temperature profiles at different points of the slab of steel are shown in Figure 10. In this case, the model and experimental results are also found to be in good agreement. A small difference is observed during the second rise in temperature. This can be explained by the calamine coat formed on the slab surface when it was introduced into the furnace for the second time, after facing the ambient air when it was taken out of the furnace.

The model accuracy is clearly validated in simulating temperature profiles in different points of the furnace. Because of the presence of high temperatures inside

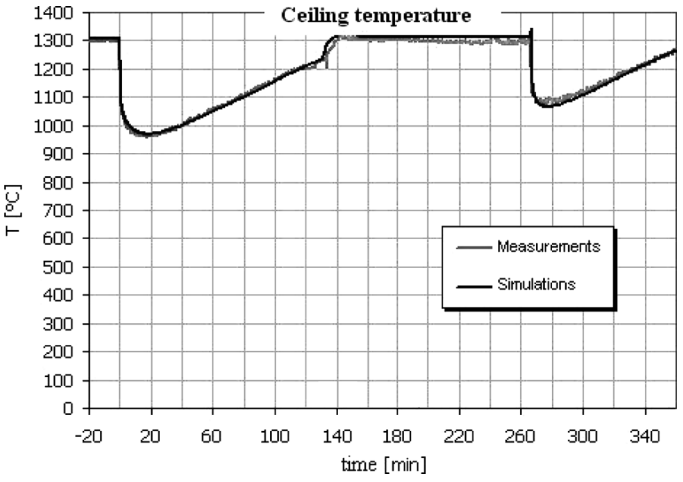

Figure 9. Temperature evolution of the furnace ceiling.

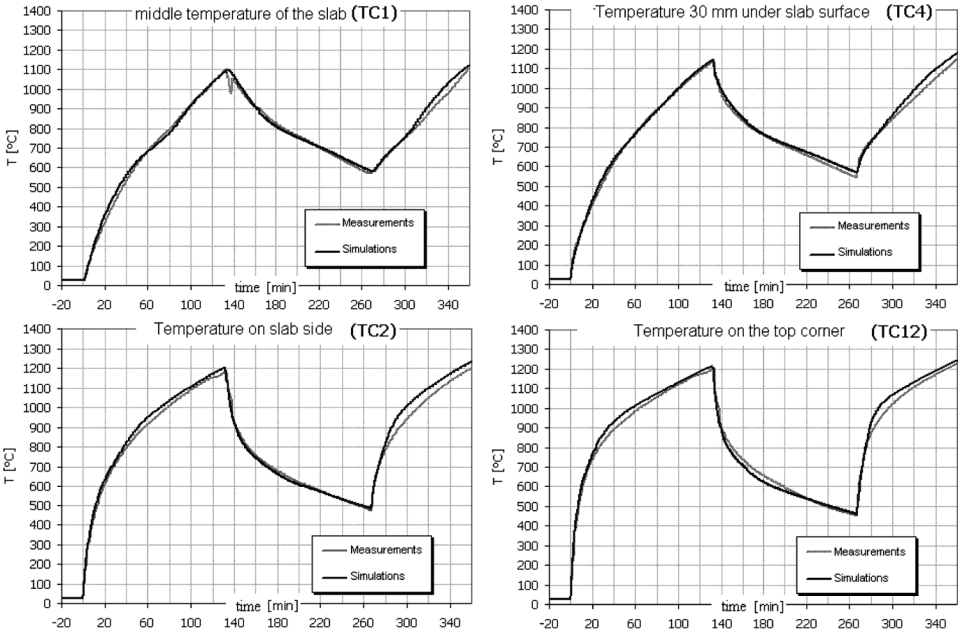

Figure 10. Temperature evolutions in some points of the slab.

the region, the heat transfer in the furnace is dominated by radiation heat transfers. The accuracy of simulations is then directly dependent on that of the radiation heat exchange factors. From the current results, we can conclude that simulated heat balances inside the furnace were in good agreement with the experiments. This demonstrates the accuracy of MODRAY, and thus of MACZM code.

CONCLUSION

The multiple absorption coefficient zonal method (MACZM) has been combined together with a set of mean beam length based on neural network correlations. Another computational method, MODRAY, is also described. The accuracy of these approaches has been demonstrated in two steps. First, MODRAY and MACZM are applied simultaneously for elementary calculations and results are compared with numerically calculated exchange factors, tabulated by Yuen and Takara. Values are shown to be in good agreement. Second, a flameless oxidation burner furnace application has been considered. The direct exchange factors in the furnace were generated simultaneously by MACZM code and MODRAY, and compared. Heat transfer in the furnace has then been simulated using a finite-volume approach. Results are validated experimentally and the temperature profiles and heat balances are found to be in good agreement with simulation results. The accuracy of MACZM code is then demonstrated.

It should be noted that MACZM is developed to be accurate in nonisothermal inhomogeneous media [14]. MACZM is thus useful for simulating accurately

non-continuous media applications, such as multi-phase mixtures and high temperature furnaces. The short calculation time makes the work of high interest for applications where media properties are varying with time and a short calculation time is needed for radiative transfer factors during transient calculations. For example, MACZM will be used to analyze a continuous industrial steel reheating furnace with moving slabs. Results of this and other transient applications using MACZM will be presented in future work.

REFERENCES

1. A. Ratzel, and J. R. Howell, Two-Dimensional Energy Transfer in Radiatively Participating Media with Conduction by the P-N Approximation, *Proc. 7th Int. Heat Transfer Conf.*, Munich, vol. 2, pp. 535–450, 1982.
2. S. Chandrasekhar, *Radiative Transfer*, Dover, New York, 1960.
3. W. A. Fiveland, Discrete Ordinate Methods for Radiative Heat Transfer in Isotropically and Anisotropically Scattering Media, *J. Heat Transfer*, vol. 109, pp. 809–812, 1987.
4. G. Krishnamoorthy, R. Rawat, and P. J. Smith, Parallel Computations of Radiative Heat Transfer using the Discrete Ordinates Method, *Numer. Heat Transfer B*, vol. 47, pp. 19–38, 2004.
5. S. H. Kim and K. Y. Huh, Assessment of the Finite-Volume Method and the Discrete Ordinate Method for Radiative Heat Transfer in a Three-Dimensional Rectangular Enclosure, *Numer. Heat Transfer B*, vol. 35, pp. 85–112, 1999.
6. G. D. Raithby and E. H. Chui, A Finite-Volume Method for Predicting a Radiant Heat Transfer in Enclosures with Participating Media, *J. Heat Transfer*, vol. 112, pp. 415–423, 1990.
7. G. D. Raithby, Discussion of the Finite-Volume Method for Radiation and its Application using 3D Unstructured Meshes, *Numer. Heat Transfer B*, vol. 35, pp. 389–405, 1999.
8. J. R. Howell, The Monte Carlo Method in Radiative Heat Transfer, *J. Heat Transfer*, vol. 120, pp. 547–560, 1998.
9. D. V. Walters and R. O. Buckius, Monte Carlo Method for Radiative Heat Transfer in Scattering Media, *Ann. Rev. of Heat Transfer*, vol. 5, pp. 131–176, 1994.
10. F. C. Lockwood and N. G. Shah, A New Radiation Solution Method for Incorporation in General Combustion Prediction Procedures, *Symp. (Int.) on Combustion*, vol. 18, pp. 1405–1414, 1981.
11. H. C. Hottel and A. F. Sarofim, *Radiative Transfer*, McGaw-Hill, New York, 1967.
12. J. J. Nobel, The Zone Method: Explicit Matrix Relations for Total Exchange Areas, *Int. J. Heat Mass Transfer*, vol. 18, pp. 261–269, 1975.
13. W. W. Yuen and E. E. Takara, The Zonal Method: A Practical Solution Method for Radiative Transfer in Nonisothermal Inhomogeneous Media, *Ann. Rev. of Heat Transfer*, vol. 8, pp. 153–215, 1997.
14. W. W. Yuen, The Multiple Absorption Coefficient Zonal Method (MACZM), An Efficient Computational Approach for the Analysis of Radiative Heat Transfer in Multidimensional Inhomogeneous Nongray Media, *Numer. Heat Transfer*, vol. 49, pp. 89–103, 2006.
15. W. W. Yuen, Definition and Evaluation of Mean Beam Lengths for Applications in Multidimensional Radiatve Heat Transfer: A Mathematically Self-Consistent Approach, *J. Heat Transfer*, vol. 130, issue 11, p. 114507, 2008.
16. G. El Hitti, M. Nemer, K. El Khoury, and D. Clodic, Modified Zonal Method for Thin Semi-transparent Media with Reflective Boundary, Proc. HT2007, Vancouver, Canada, 32033, *ASME-JSME*, vol. 1, pp. 395–401, 2007.

17. L. Ferrand, Modélisation et Expérimentation des Fours de Réchauffage Sidérurgiques Equipés de Bruleurs Régénératifs à Oxydation sans Flamme, Ph.d. thesis, ENSMP, Paris, 2003. (In French.)
18. A. F. Emery, O. Johansson, and A. Abrous, Radiation Heat Transfer Shapefactors for Combustion Systems Fundamentals and Applications of Radiation Heat Transfer, *ASME HTD*, vol. 72, pp. 119–126, 1987.
19. D. K. Edwards, The Plating Algorithm for Radiation Script-F Transfer Factor, *J. Heat Transfer*, vol. 108, pp. 237–238, 1986.
20. G. El Hitti, M. Nemer, and K. El Khoury, Reducing CPU Time for Radiative Exchange and Transient Heat Transfer Analysis using Zone Method, *Numer. Heat Transfer, B*, vol. 56, pp. 23–37, 2009.
21. G. El Hitti, M. Nemer, K. El Khoury, and D. Clodic, The Rating Algorithm for Radiation Total Exchange Area Calculation, *Numer. Heat Transfe B*, vol. 57, pp. 110–125, 2010.